ON DISSIPATIVE MHD MIXED CONVECTION BOUNDARY-LAYER FLOW OF JEFFREY FLUID OVER AN INCLINED STRETCHING SHEET WITH NANOPARTICLES: Buongiorno Model

by

Syazwani MOHD ZOKRI[a], Nur Syamilah ARIFIN[a], Abdul Rahman MOHD KASIM[a] and Nurul Farahain MOHAMMAD[b], and Mohd Zuki SALLEH[a*]

[a] Faculty of Industrial Sciences and Technology, Universiti Malaysia Pahang, Kuantan, Pahang, Malaysia
[b] Deptartment of Computational and Theoretical Sciences, Kulliyyah of Science, International Islamic University Malaysia, Kuantan, Pahang, Malaysia

Original scientific paper
https://doi.org/10.2298/TSCI171120178M

Present paper utilizes a combination of non-Newtonian fluid model (Jeffrey fluid) with Buongiorno model (nanofluid). The Jeffery fluid, which is regarded as a base fluid, together with suspended nanoparticles are examined over an inclined stretching sheet with the amalgamated impacts of mixed convection and viscous dissipation. The mathematical formulation of this model is done by choosing the appropriate similarity variables for the aim to reduce the complexity of governing partial differential equations. The Runge-Kutta-Fehlberg (RKF45) method is then applied to the resulting of non-linear ODE to generate numerical results for highlighting the impact of emerging parameters towards specified distributions. Both the graphical and tabular representations of vital engineering physical quantities are also shown and deliberated. For the increase of Eckert number, thermophoresis diffusion, and Brownian motion parameters, the elevation of temperature profiles is observed. Besides, the thermophoresis diffusion parameter tends to accelerate the nanoparticle concentration profile while Brownian motion parameter displays the opposite behavior.

Key words: *Jeffrey nanofluid, prescribed wall temperature, viscous dissipation, inclined stretching sheet, Buongiorno model*

Introduction

The enlargement in industrial and technological applications has increased the need for knowledge on the concept of heat and mass transfer, particularly on the non-linear rheological fluid. In fact, this concept is vital as it contributes to the success of numerous engineering applications. These engineering applications may consist of the manufacturing of plastic and rubber sheets, production of glass fibers, extrusion process, polymer technology *etc.* Recent investigations have shown that the non-linear rheological fluid had received extra attention [1-5]. This is due to the complex nature of fluid used in most industrial applications, that a single constitutive equation is inadequate to describe such fluids. Differs to Newtonian fluid, the connection between the rate of stress and strain is non-linear because of dependency of

* Corresponding author, e-mail: zuki@ump.edu.my

fluid viscosity on time or deformation. According to the literature, many non-Newtonian fluids have been proposed; yet, each of them displays dissimilar characteristics. Therefore, examining these fluids entirely at one time is slightly impossible. In view of the special ability in explaining the physical characteristics of both relaxation and retardation times, the Jeffrey fluid model has been picked for further research. Thorough investigations related to this fluid model include those of Dalir [6], Hayat *et al.* [7], Narayana and Babu [8], Ojjela *et al.* [9], Hayat *et al.* [10], and Hayat *et al.* [11].

It is known that nanofluids are the solid-liquid composite materials containing suspended nanoparticles such as oxides, metals, nitrides, carbides, or nonmetals, *i. e.* graphite and carbon nanotubes with diameter between 1 and 100 nm. The properties of the base fluid, such as water or ethylene glycol are conceivably enhanced by mixing it with nanoparticles; nonetheless, subjected to the particle's shape, size and the base fluid itself [12]. Here, the presence of nanoparticles is significant as it can strongly enhance the thermal properties as well as is highly potential to the rate of heat exchange with no drop in pressure. Moreover, the Brownian motion and thermophoresis diffusion are liable on the enhancement of the thermal performance [13]. Accordingly, nanofluids have undeniably become a subject of interest to be studied. A comparison study on the combination of ethylene glycol with copper nanoparticles and pure ethylene glycol or ethylene glycol with oxide nanoparticles was explored by Eastman *et al.* [14] to examine the thermal properties of each fluid. In comparison to the ethylene glycol with oxide nanoparticles, it is evident that the thermal properties of ethylene glycol and copper nanoparticles are greater. Choi *et al.* [15] discovered a distinguished change in the thermal performance of the base fluid as a result of dispersion of a very small quantity of nanotubes. Precisely, with 1 vol.% of nanotubes, the ratio of thermal conductivity is greater than 2.5. Khan and Pop [16] were the first who studied the numerical solution of nanofluid passing through a stretching sheet. With the aim of focusing on the same problem, Makinde and Aziz [17] extended the study to the convective boundary conditions. The stagnation point flow of power-law nanofluid from a convectively heated stretching sheet was then tackled by Ibrahim and Makinde [18]. Following the Buongiorno model, the Jeffrey fluid model with the nanoparticles were employed by Shehzad *et al.* [19], Avinash *et al.* [20], and Qayyum *et al.* [21] to investigate the influences of Jeffrey fluid, Brownian motion and themophoresis diffusion parameters.

The involvement of the traits from the forced and free flow conditions, or mixed convection flow is pronounced when the forced flow impact in the free convection or the buoyancy force impact in the forced convection, is sizable. In particular, the buoyancy parameter, $\gamma = \mathrm{Gr}/\mathrm{Re}_x^2$ confers a measure of free convection to the forced convection flows effects, where $\gamma \to 0$ signifies the dominant mode of transport for the forced convection, whereas $\gamma \to \infty$ implies the dominant mode of free convection. However, the contribution of each convections on heat transfer enhancement is reliant on the fluid-flow, temperature, orientation and surface geometry. Abbasi *et al.* [22] scrutinized the mixed convection flow with thermal radiation and double stratification effects in MHD Jeffrey nanofluid induced by stretching sheet. They noted that the changes in the temperature profile for the smaller values of mixed convection parameter was still significant compared to the concentration buoyancy parameter. In other work, Dhanai *et al.* [23] inspected the impacts of velocity and thermal slip past an inclined cylinder with mixed convection. Aided by the Runge-Kutta-Fehlberg method together with shooting technique, the free convection flow was revealed to be more effective than the forced convection flow for larger value of mixed convection parameter, and this implies a rise to the fluid-flow.

The MHD reflects the science of the motion of electrically conducting fluids under magnetic fields. Conceptually, magnetic fields can instigate currents in a moving conductive fluid, that result in the polarization of fluid and concurrently modify the magnetic field. This situation is principally one of the reciprocal contacts between the motion of fluid and the magnetic field; the fluid-flow alters the magnetic field and vice versa. Problem concerning the heat transfer and electrically conducting flow past a stretching sheet has turned into one of the most favorable discussed topics. The paramount interest of the topic can be affiliated to the continuously growing industrial applications, specifically in the productions of cable coatings, glassware, paper, fabrications of adhesive tapes, metal spinning, metallic plates and fine-fiber mats. The stretching and cooling processes of such industrial applications need to be controlled to achieve desirable manufactured products. In essence, the manufacturing process requires both the thermal and mechanical interactions of stretched surface with the ambient fluid. A pioneering study was conducted by Sakiadis [24] on the boundary-layer flow over a continuously moving surface. The flow past a stretching plate was subsequently enquired into by Crane [25]. Henceforth, various researchers elongated this research area by addressing different surface geometry with several effects [26-29]. However, the current study will be restricted to the inclined stretching sheet. Reddy [30] discussed the combined impacts of thermal radiation and chemical reaction in MHD Casson fluid past an exponentially inclined permeable stretching sheet. Afridi *et al.* [31] examined the impact of entropy generation in a viscous fluid from an inclined stretching sheet. Approximate analytical approach, namely homotopy analysis method was executed by Sravanthi [32] to observe the influences of suction/blowing, Soret and Dufour and thermal radiation over an exponentially inclined stretching sheet. Other distinguished explorations allied with the inclined stretching sheet were published by Thumma *et al.* [33] and Gupta *et al.* [34].

A noteworthy effect of viscous dissipation is discerned in the case of highly viscous fluid or when the fluid-flows very fast. Heat is basically generated from the frictional force induced by the shear in the fluid-flow. Soundalgekar [35] studied the viscous dissipation effect with constant suction due to a vertical porous plate. The same effect was then considered by Yirga and Shankar [36], Mohamed *et al.* [37, 38], and Besthapu *et al.* [39] in a nanofluid past a stretching sheet, horizontal circular cylinder and exponentially stretching sheet, respectively. Meanwhile, Hussain *et al.* [40] addressed this effect from a stretching cylinder embedded in the MHD Sisko nanofluid. Recently, the combined effects of viscous dissipation and Joule heating were scrutinized by Kumar *et al.* [41] and Mahanthesh and Gireesha [42] in the respective ferro-nanofluid and two phase flow of Casson fluid.

Based on the aforementioned investigations, it is ascertainable that no endeavours has been effectuated on the impact of viscous dissipation in MHD mixed convection Jeffrey fluid with nanoparticles due to the inclined stretching sheet. The model of Jeffrey fluid is herein considered as a base fluid. With the succor of MAPLE package, the RKF45 method is embarked upon to solve the highly non-linear ODE. The impacts of emerging parameters towards specified distributions are highlighted in the graphical and tabular forms. As yet, there has been no prevailing study published on this topic, thus the authors acknowledge this work as new.

Problem formulation

A steady, 2-D and laminar flow of mixed convection boundary-layer flow in an electrically conducting Jeffrey nanofluid past an inclined stretching sheet with an inclination angle, α_0, to the vertical is deliberated. Here, the velocity of the stretching sheet is considered linear, *i. e.* $u_w(x) = ax$ (a is constant and $a > 0$). The stretched surface of temperature and

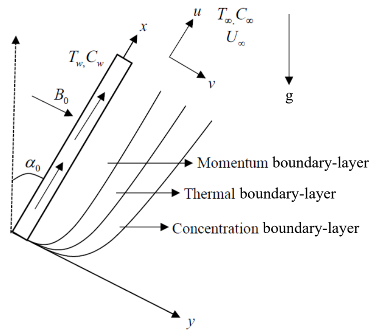

Figure 1. Schematic diagram

nanoparticle concentrations is further considered to be greater than the free stream of temperature and nanoparticle concentration where $T_w(x) > T_\infty$ and $C_w(x) > C_\infty$, respectively. The transverse magnetic field, B_0, is imposed perpendicularly to the stretched surface. Figure 1 displays the schematic diagram of the problem, in which x- and y-axes are directed in the same direction of the flow field and normal to it, respectively. To obtain the self-similarity equation, the thermal and nanoparticle concentration expansion coefficients are assumed to be $\beta_T = mx^{-1}$ and $\beta_C = nx^{-1}$, whereby m and n are constants [43, 44] while the temperature and nanoparticle concentration of the stretching sheet are $T_w(x) = T_\infty + bx^2$ and $C_w(x) = C_\infty + dx^2$, where b and d are constants [31, 45]. The governing equations of Jeffrey nanofluid can be expressed [6, 22]:

$$\frac{\partial u}{\partial x} + \frac{\partial v}{\partial y} = 0 \tag{1}$$

$$u\frac{\partial u}{\partial x} + v\frac{\partial u}{\partial y} = \frac{\nu}{1+\lambda}\left[\frac{\partial^2 u}{\partial y^2} + \lambda_1\left(\frac{\partial u}{\partial y}\frac{\partial^2 u}{\partial x \partial y} + u\frac{\partial^3 u}{\partial x \partial y^2} - \frac{\partial u}{\partial x}\frac{\partial^2 u}{\partial y^2} + v\frac{\partial^3 u}{\partial y^3}\right)\right] - \frac{\sigma B_0^2}{\rho_f}u +$$
$$+\left[\beta_T \rho_f (T - T_\infty) + \beta_C (C - C_\infty)\right]\mathrm{g}\cos\alpha_0 \tag{2}$$

$$u\frac{\partial T}{\partial x} + v\frac{\partial T}{\partial y} = \alpha\frac{\partial^2 T}{\partial y^2} + \tau\left[D_B\frac{\partial C}{\partial y}\frac{\partial T}{\partial y} + \frac{D_T}{T_\infty}\left(\frac{\partial T}{\partial y}\right)^2\right] +$$
$$+\frac{\nu}{C_p(1+\lambda)}\left[\left(\frac{\partial u}{\partial y}\right)^2 + \lambda_1\left(u\frac{\partial u}{\partial y}\frac{\partial^2 u}{\partial x \partial y} + v\frac{\partial u}{\partial y}\frac{\partial^2 u}{\partial y^2}\right)\right] \tag{3}$$

$$u\frac{\partial C}{\partial x} + v\frac{\partial C}{\partial y} = D_B\frac{\partial^2 C}{\partial y^2} + \frac{D_T}{T_\infty}\frac{\partial^2 T}{\partial y^2} \tag{4}$$

The associated boundary conditions are:

$$\begin{gathered} u = u_w(x) = ax,\ v = 0,\ T = T_w(x) = T_\infty + bx^2,\ C = C_w(x) = C_\infty + dx^2 \ \text{ at } y = 0 \\ u \to 0,\ v \to 0,\ T \to T_\infty,\ C \to C_\infty \ \text{ as } y \to \infty \end{gathered} \tag{5}$$

From the equations, the respective velocity components in the x- and y-directions are written as u and v while $\alpha, \mathrm{g}, \nu, \sigma, \rho_f, \lambda, \lambda_1, T, C, C_p, D_B, D_T$ being the respective thermal diffusivity, gravitational acceleration, kinematic viscosity, electrical conductivity, density of fluid, ratio of relaxation to retardation times, retardation time, fluid temperature, nanoparticle concentration of the fluid, specific heat capacity, Brownian motion, and thermophoretic diffusion parameters. In addition, let $\tau = (\rho c)_p / (\rho c)_f$ be the ratio of nanoparticle heat capacity to the base fluid heat capacity. The following similarity transformation variables are imposed in order to reduce the complexity of eqs. (1)-(4) [16, 22],

$$\eta = (a/\nu)^{1/2} y, \quad u = axf'(\eta), \quad v = -(a\nu)^{1/2} f(\eta),$$
$$\theta(\eta) = (T - T_\infty)/(T_w - T_\infty), \quad \phi(\eta) = (C - C_\infty)/(C_w - C_\infty) \tag{6}$$

On account of the transformations, eq. (1) is inevitably satisfied and eqs. (2)-(4) become:

$$f''' + \lambda_2(f''^2 - ff^{(iv)}) - (1+\lambda)(f'^2 - ff'') - (1+\lambda)Mf' + (1+\lambda)\gamma(\theta + N\phi)\cos\alpha_0 = 0 \tag{7}$$

$$(1+\lambda)\theta'' + (1+\lambda)\Pr(f\theta' - 2f'\theta + Nb\theta'\phi' + Nt\theta'^2) +$$
$$+ \mathrm{Ec}\Pr[f''^2 + \lambda_2 f''(f'f'' - ff''')] = 0 \tag{8}$$

$$\phi'' + Le\Pr\left(f\phi' - 2f'\phi\right) + \left(Nt/Nb\right)\theta'' = 0 \tag{9}$$

subject to the boundary conditions:

$$f(0) = 0, \quad f'(0) = 1, \quad \theta(0) = 1, \quad \phi(0)=1$$
$$f'(\infty) \to 0, \quad f''(\infty) \to 0, \quad \theta(\infty) \to 0, \quad \phi(\infty) \to 0 \tag{10}$$

The dimensionless parameters arising in eqs. (7)-(9) are: $\Pr = \nu/\alpha$ – the Prandtl number, $\gamma = GR/\mathrm{Re}_x^2 = \mathrm{g}\beta_T(T_w - T_\infty)x/u_w^2$ – the mixed convection parameter, $M = \sigma B_0^2/\rho_f a$ – the magnetic parameter, $\lambda_2 = \lambda_1 a$ – the Deborah number, $\mathrm{Le} = \alpha/D_B$ – the Lewis number, $N = \beta_C(C_w - C_\infty)/\beta_T(T_w - T_\infty)$ – the concentration buoyancy parameter, $Nb = (\rho C)_p D_B \cdot (C_w - C_\infty)/(\rho C)_f \nu$ – the Brownian motion parameter, $\mathrm{Ec} = u_w^2/C_p(T_w - T_\infty)$ – the Eckert number, and $Nt = (\rho C)_p D_T(T_w - T_\infty)/(\rho C)_f \nu T_\infty$ – the thermophoresis diffusion parameter. The exact solution of eq. (7) when $M = \gamma = 0$ is given as [7]:

$$f(\eta) = (1 - \mathrm{e}^{-r\eta})/r \tag{11}$$

where $r = [(1+\lambda)/(1+\lambda_2)]^{1/2}$. The reupon, $f''(\eta) = -r\mathrm{e}^{-r\eta}$ denotes the second derivative of eq. (11). At the surface of the sheet, the gradient of velocity is:

$$f''(0) = -r \tag{12}$$

The requisite engineering physical quantities such as the local skin friction coefficient, Nusselt number and Sherwood number are:

$$C_f = \frac{\tau_w}{\frac{1}{2}\rho_f u_w^2(x)}, \ \mathrm{Nu}_x = \frac{xq_w}{k(T_w - T_\infty)} \ \text{and} \ \mathrm{Sh}_x = \frac{xq_m}{D_B(C_w - C_\infty)} \tag{13}$$

where

$$\tau_w = \frac{\mu}{1+\lambda}\left[\frac{\partial u}{\partial y} + \lambda_1\left(u\frac{\partial^2 u}{\partial x \partial y} + v\frac{\partial^2 u}{\partial y^2}\right)\right]_{y=0}, \quad q_w = -k\left.\frac{\partial T}{\partial y}\right|_{y=0}, \quad \text{and} \quad q_m = -D_B\left.\frac{\partial C}{\partial y}\right|_{y=0}$$

are the shear stress, surface heat flux, and surface mass flux, respectively. The reduced engineering physical quantities which consist of skin friction coefficient, Nusselt number and Sherwood number are:

$$C_f \operatorname{Re}_x^{1/2} = \frac{2}{1+\lambda}\left[f''(0) + \lambda_2 f''(0)\right], \quad \operatorname{Nu}_x \operatorname{Re}_x^{-1/2} = -\theta'(0), \text{ and } \operatorname{Sh}_x \operatorname{Re}_x^{-1/2} = -\phi'(0) \quad (14)$$

where the local Reynolds number is defined as $\operatorname{Re}_x = u_w x/\nu$.

Particular case: In the nonappearance of mixed convection parameter $\gamma = 0$ and magnetic parameter $M = 0$, the present solution of momentum eq. (7) excellently coincides with that of Dalir [6], whose results are congruous with the exact solution of eq. (12). Besides, eqs. (7) and (8) are reduced to the Newtonian model proposed by Afridi *et al.* [31], provided that the absenteeism of the following parameters: $\lambda = \lambda_2 = N = Nb = Nt = \text{Le} = 0$.

Numerical procedure

Equations (7)-(9) together with boundary conditions (10) are solved numerically using the RKF45 method with the aid of MAPLE package. This method implicates the transformation of eqs. (7)-(9) into first order system by supposing $(f, f', f'', f''', \theta, \theta', \phi, \phi') = (Z_1, Z_2, Z_3, Z_4, Z_5, Z_6, Z_7, Z_8) = Z$, as presented below [23, 46]:

$$\begin{pmatrix} Z_1' \\ Z_2' \\ Z_3' \\ Z_4' \\ Z_5' \\ Z_6' \\ Z_7' \\ Z_8' \end{pmatrix} = \begin{pmatrix} Z_2 \\ Z_3 \\ Z_4 \\ \dfrac{1}{Z_1}\left\{Z_3^2 - \dfrac{1}{\lambda_2}\left[(1+\lambda)(Z_2^2 - Z_2 Z_3) + (1+\lambda)M Z_2 - (1+\lambda)\gamma(Z_5 + N Z_7)\cos\alpha_0 - Z_4\right]\right\} \\ Z_6 \\ -\Pr\left(Z_1 Z_6 - 2 Z_2 Z_5 + Nb Z_6 Z_8 + Nt Z_6^2\right) - \dfrac{\text{Ec}\Pr}{(1+\lambda)}\left[Z_3^2 + \lambda_2 Z_3\left(Z_2 Z_3 - Z_1 Z_4\right)\right] \\ Z_8 \\ -\text{Le}\Pr\left(Z_1 Z_8 - 2 Z_2 Z_7\right) + \left(\dfrac{Nt}{Nb}\right) Z_6' \end{pmatrix} \quad (15)$$

with the initial conditions:

$$Z^T = (0,\ 1,\ Z_3,\ Z_4,\ 1,\ Z_6,\ 1,\ Z_8)^T \quad (16)$$

The system utilizes the Newton-Raphson method and shooting method to guess the missing initial conditions, Z_3, Z_4, Z_6, and Z_8 *i. e.* $f''(0)$, $f'''(0)$, $\theta'(0)$, and $\phi'(0)$ by an iterative process until the boundary conditions are satisfied. The convergence criteria is fixed to be 10^{-9}, while the boundary-layer thickness is set from $\eta_\infty = 5$ to 10 to acquire the asymptotic behaviours of velocity, temperature and concentration profiles.

Results and discussion

A comprehensive solution of the dimensionless parameters on the velocity $f'(0)$, temperature, $\theta(0)$, and nanoparticle concentration $\phi(0)$ profiles as well as the reduced skin friction coefficient, $C_f \operatorname{Re}_x^{1/2}$, Nusselt number, $\operatorname{Nu}_x \operatorname{Re}_x^{-1/2}$, and Sherwood number, $\operatorname{Sh}_x \operatorname{Re}_x^{-1/2}$, are demonstrated through figs. 2-19 and tabs. 1(a) and 1(b). The default parameters used throughout the research are $\lambda = 0.1$, $\lambda_2 = 0.2$, $\Pr = 1.0$ (electrolyte solution), $Nb = Nt = N = \gamma = 0.3$, $\alpha_0 = \pi/4$, $M = \text{Le} = 0.7$, and Ec = 0.2, except otherwise mentioned [27, 47]. Precision of the present codes is guaranteed by comparing the current results with some related existing publications as presented in tab. 1. The comparative study has shown a splendid consistency; thus, the analysis of results can now be proceeded.

Table 1(a). Comparative values of $f''(0)$ for some values of λ_2 when $\lambda = 0.2$, $M = \gamma = 0$

λ_2	Exact solution of eq. (12)	[6]	Present
0.0	–1.09544512	–1.09641580	–1.09544512
0.4	–0.92582010	–0.92724220	–0.92582010
0.8	–0.81649658	–0.81808091	–0.81649658
1.0	–0.77459667	–0.77618697	–0.77459667

Table 1(b). Comparative values of $\theta'(0)$ for some values of Pr and Ec when $\lambda = \lambda_2 = Nb = Nt = N = \mathrm{Le} = 0$, $M = 1.0$, $\gamma = 0.2$, $\alpha_0 = \pi/4$, Ec = 1.0, and Pr = 1.2

Pr	[31]	Present	Ec	[31]	Present
0.3	0.3897	0.38979158	0.0	1.3873	1.38740227
0.7	0.6219	0.62191866	0.3	1.2125	1.21260213
1.2	0.8106	0.81061315	0.6	1.0393	1.03934047
1.5	0.8962	0.89621903	0.9	0.8675	0.86758366

Figures 2-7 depict the changes in the velocity profile $f'(\eta)$ *vs.* η for several parameters such as λ, λ_2, M, γ, N, and α_0, respectively. Figure 2 shows a manifest result that a rise in λ tends to decelerate the flow of fluid. The reduction in fluid motion is caused by the domination of relaxation time (time needed for the material to maintain its original position) in comparison to the retardation time (time needed for the material to react to distortion). This has offered more resistance to the fluid-flow and correspondingly, the thickness of momentum boundary-layer is lessened. In relation to the increment of λ_2 on the velocity profile, the flow of fluid and the thickness of momentum boundary-layer are observed to rise as drawn in fig. 3. Referring to the definition of λ_2, *i. e.* $\lambda_2 = \lambda_1 a$, it is patented that λ_2 and λ_1 are proportional to one another, where a rise in λ_2 is strongly influenced by the development in the λ_1. The

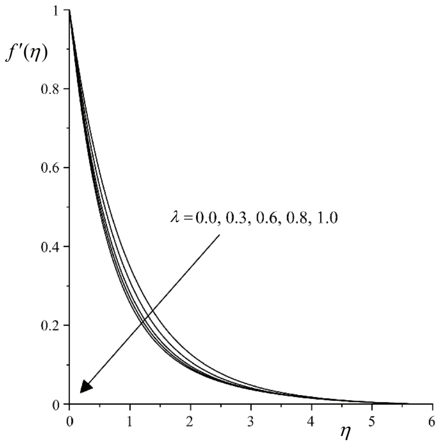

Figure 2. Impact of λ on $f'(\eta)$

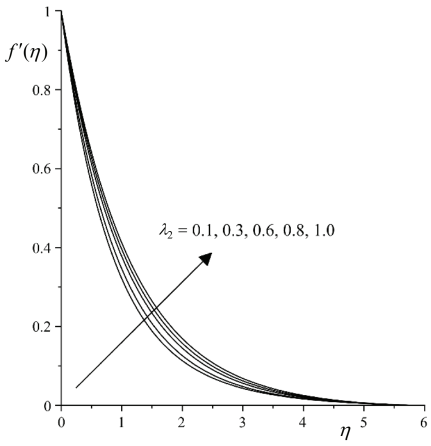

Figure 3. Impact of λ_2 on $f'(\eta)$

involvement of λ_1 replicates that the fluid needs to reach an equilibrium state in response to the applied force. Accordingly, the increase in λ_1 aids in the increment of λ_2, which then promotes the enhancement of velocity profile. Furthermore, λ_2 can also measure the elasticity of the materials and highly elastic fluid is associated with higher λ_2. For small λ_2, the fluid behaves in a viscous manner and this accounts to the quick convergent of momentum boundary-layer thickness. In fig. 4, the parameter M is investigated to measure the outcome of magnetic field strength on the fluid motion. Physically, higher M implies the stronger magnetic field. That being the case, this will induce the Lorentz force, which is known as the resistive type force or drag force that functions to resist the motion of fluid, so as to decrease the profile for velocity. Figure 5 portrays the influence of several values of γ on the velocity profile. From the figure, it is witnessed that the profile for velocity is a growing function of γ. As a matter of fact, γ is depending on the buoyancy force. The increase in γ induces the buoyancy force on the external flow, henceforth creates a pleasing pressure gradient that elevates the flow of fluid. Similar trend of graph is noticed in fig. 6, where the impact of N has accelerated the fluid-flow. This situation emerges due to the domination of buoyancy forces over the viscous forces. Buoyancy force has a propensity to speed up the fluid motion, which leads to the augmentation of velocity profile and its associated momentum boundary-layer thickness. Besides, fig. 7 illustrates the opposite behavior of the inclination angle α_0, which is in the range of acute angles, *i. e.* 0 to $\pi/2$. As α_0 raises, the fluid-flow is seen to deteriorate. This is due to the decrement of buoyancy ratio strength in the momentum equation, $[\beta_T(T-T_\infty)+\beta_C(C-C_\infty)]\mathrm{g}\cos\alpha_0$. Evidently, when $\alpha_0=\pi/2$, the stretched sheet is directed horizontally, and the buoyancy force does no longer exist due to the absence of buoyancy ratio term. Meanwhile, when $\alpha_0=0$, the sheet is oriented vertically, and the maximum buoyancy force transpires. Thence, in comparison to the horizontal surface $(\alpha_0=\pi/2)$, it can be deduced that the fluid-flow is higher for the case of vertical surface $(\alpha_0=0)$.

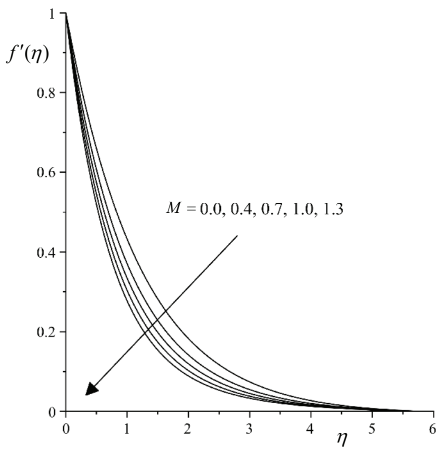

Figure 4. Impact of *M* on $f'(\eta)$

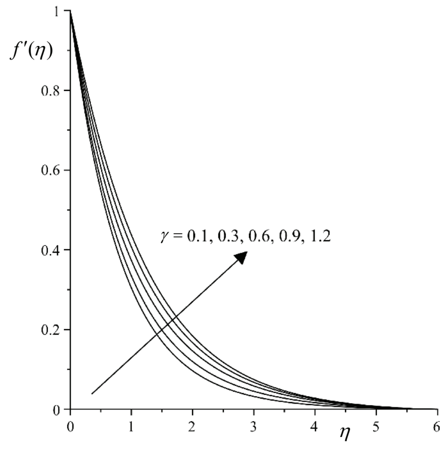

Figure 5. Impact of γ on $f'(\eta)$

Figures 8-12 elucidate the impact of the Ec, Nt and Nb on the profiles of temperature $\theta(\eta)$ and nanoparticle concentration $\phi(\eta)$, respectively. Clearly, fig. 8 shows that the temperature profile is significantly influenced by Eckert number. In view of physical meaning, Eckert number characterizes the relative contribution of kinetic energy at the wall to the specific enthalpy difference between the wall and the fluid. Escalating the viscous dissipation effect

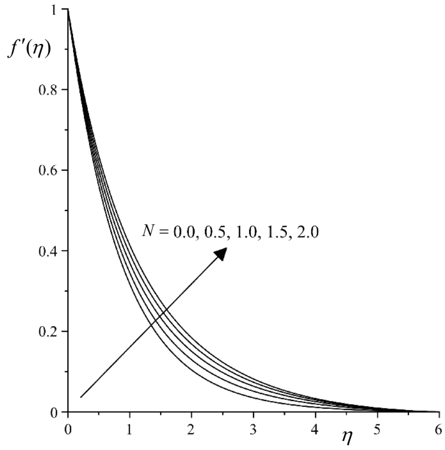

Figure 6. Impact of N on $f'(\eta)$

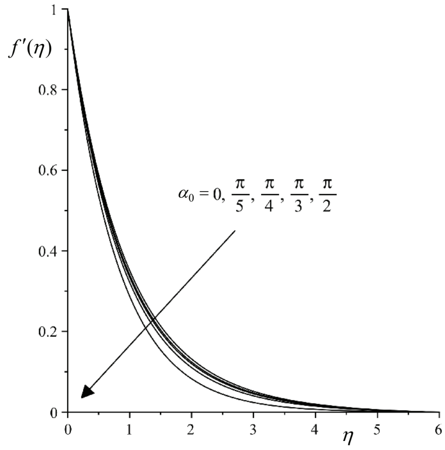

Figure 7. Impact of α_0 on $f'(\eta)$

on fluid-flow enhances the kinetic energy as well as elevates the temperature profile and thermal boundary-layer thickness. Figures 9 and 10 measure the changes of Nt towards the temperature and nanoparticle concentration profiles, in which both profiles are the rising function of Nt. The increment is affiliated to the mobile particles near the hot surface which create a thermophoretic force; a force where the motion of nanoparticles is induced by the temperature gradient. It follows that the nanoparticles are blown away from the hot surface of the stretched sheet and a relatively particle-free layer close to the sheet is formed subsequently [5]. On that account, the distribution of nanoparticles becomes strengthen, thereby reinforcing the temperature and nanoparticle concentration profiles. Moreover, it is observed that the graph for temperature is insignificantly varied compared to the nanoparticle concentration. The reason is because Nt is a nanoscale parameter, hence its impact on the temperature is relatively fewer. The consequence of Nb on both temperature and nanoparticle concentration profiles are revealed in figs. 11 and 12. It is crucial to mention that a larger Nb corresponds to higher molecular diffusion with lower viscosity. Increasing Nb will reinforce the collision amongst the

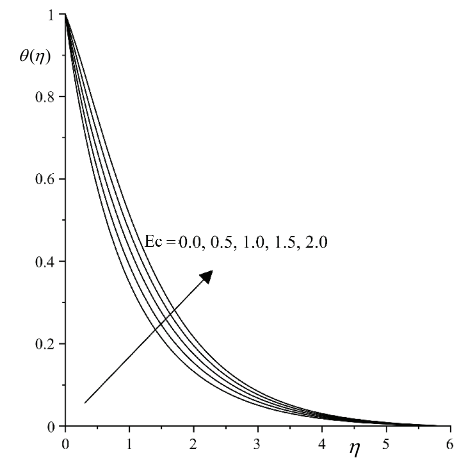

Figure 8. Impact of Ec on profile $\theta(\eta)$

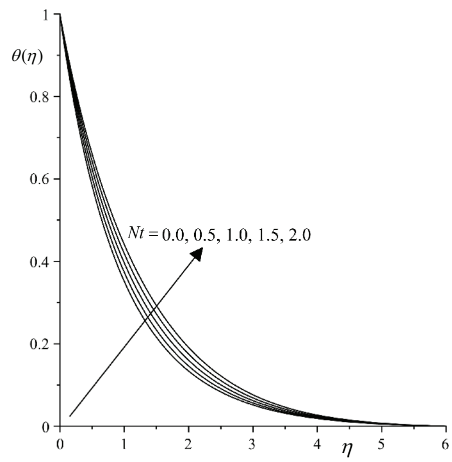

Figure 9. Impact of Nt on $\theta(\eta)$

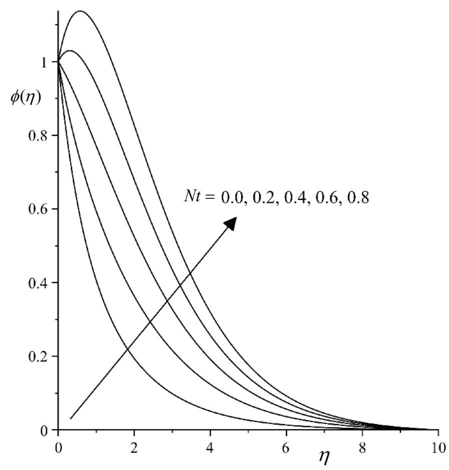

Figure 10. Impact of *Nt* on $\phi(\eta)$

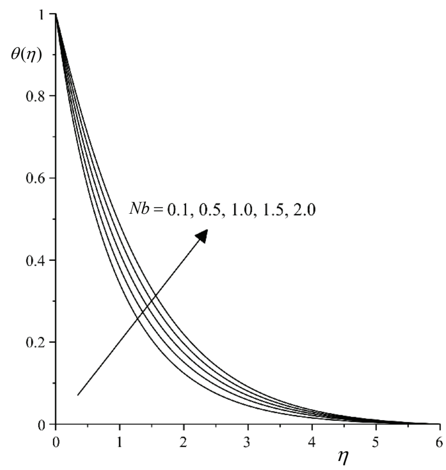

Figure 11. Impact of *Nb* on $\theta(\eta)$

molecules of fluid and its zig zag motion. Such reinforcement has triggered the production of extra heat in the fluid as well as intensified the fluid thermal conductivity, which then prevails upon the increment of temperature and decrement of nanoparticle concentration. In addition, as suggested in many theoretical studies, the Brownian motion of nanoparticles may boost up the thermal conduction through one of the following ways: either the transport of heat on fluid-flow by direct effect of nanoparticles, or an indirect effect of individual nanoparticles attributable to the micro-convection of fluid [48].

Figure 13 is enlisted to study the effect of Lewis number on the nanoparticle concentration profile $\phi(\eta)$ *vs.* η. The Lewis number defines the relationship between heat and mass transfer coefficients. Mathematically, Lewis number accounts for the ratio of the Schmidt number to the Prandtl number, that heat and mass will both diffuse at an equal rate when Le = 1 and heat will diffuse even more speedily than mass when Le > 1. As such, the increase of Lewis number clearly brings forth to the diminution of nanoparticle concentration along with its related concentration boundary-layer thickness.

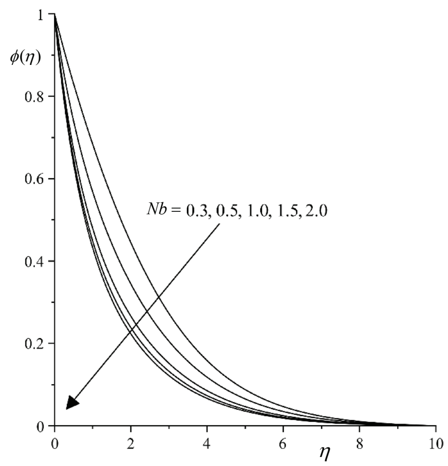

Figure 12. Impact of *Nb* on $\phi(\eta)$

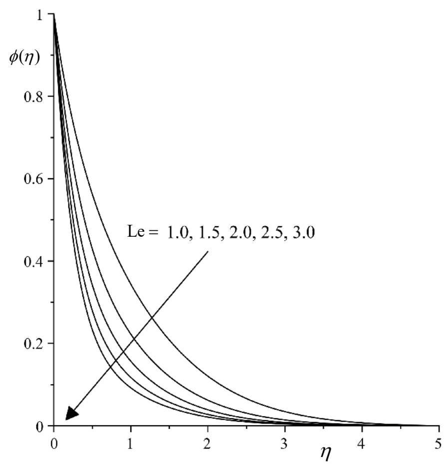

Figure 13. Impact of Le on $\phi(\eta)$

Figures 14-19 closely describe the variations of the reduced skin friction coefficient, $C_f \mathrm{Re}_x^{1/2}$, Nusselt number, $\mathrm{Nu}_x\mathrm{Re}_x^{-1/2}$, and Sherwood number, $\mathrm{Sh}_x\mathrm{Re}_x^{-1/2}$, on the diverse values of λ_2, *Nt*, and Le. Figure 14 displays the demotion of $C_f\mathrm{Re}_x^{1/2}$ corresponding to the changes occurred in λ_2 and *Nt.* More specifically, the increase in λ_2 is to lessen the $C_f\mathrm{Re}_x^{1/2}$. This is physically due to the enhancement of viscoelasticity property of materials that assists in the reduction of the wall shear stress, hence leading to the slackening of the frictional forces. Contrariwise, the increase of Nt has moderately increased the $C_f\mathrm{Re}_x^{1/2}$, and the increment is noticed to be the highest when $\lambda_2 = 0.1$. Since Nt facilitates the nanoparticles diffusion in the boundary-layer, therefore, the distribution of nanoparticles from the heated surface for $\lambda_2 = 0.1$ is manifestly more effective than $\lambda_2 = 1.0$. In figs. 15 and 16, the influences of λ_2 and Nt have considerably enhanced the $\mathrm{Nu}_x\mathrm{Re}_x^{-1/2}$ and $\mathrm{Sh}_x\mathrm{Re}_x^{-1/2}$, whereby the results are interrelated with figs. 9 and 10.

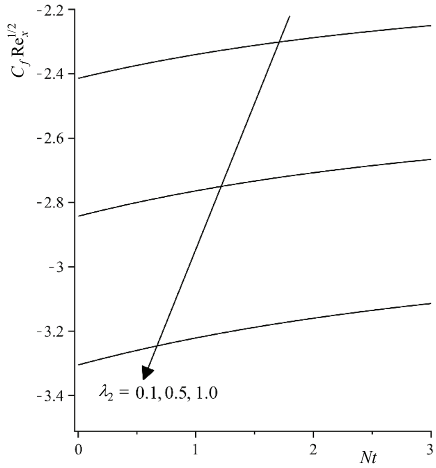

Figure 14. Impact of λ_2 and *Nt* on $C_f\mathrm{Re}_x^{1/2}$

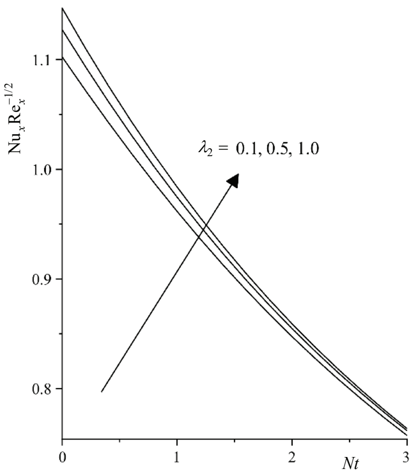

Figure 15. Impact of λ_2 and *Nt* on $\mathrm{Nu}_x\mathrm{Re}_x^{-1/2}$

These results are foreseeable as the improvement of heat and nanoparticle concentration transfer rates at the surface is predominantly caused by the higher thermal diffusivity offered from the rising Nt. As contrasted to fig. 14, it is also found that the heat and nanoparticle concentration transfer rates are highly prominent when $\lambda_2 = 1.0$. Furthermore, when the values of λ_2 and Lewis number are enhanced, the $C_f\mathrm{Re}_x^{1/2}$ is observed to be decelerating, as shown in fig. 17. In the figure, the presence of parameters λ_2 and Lewis number has reduced the friction within the fluid and between the fluid and the wall. Figures 18 and 19 demonstrate the rising effects of parameters λ_2 and Lewis number on the $\mathrm{Nu}_x\mathrm{Re}_x^{-1/2}$ and $\mathrm{Sh}_x\mathrm{Re}_x^{-1/2}$. The outcome can be precisely linked with fig. 13, wherein the escalation of heat and nanoparticle concentration transfer rates is observed in the consequence of nanoparticle boundary-layer deprivation.

The responses of several continent parameters towards the $C_f\mathrm{Re}_x^{1/2}$, $\mathrm{Nu}_x\mathrm{Re}_x^{-1/2}$, and $\mathrm{Sh}_x\mathrm{Re}_x^{-1/2}$ are provided in tabs. 2(a) and 2(b). Manifestly, the $C_f\mathrm{Re}_x^{1/2}$ becomes an increasing function of parameters λ, γ, N, Nt, and Ec whereas it is a decreasing function for λ_2, M, α_0, Pr, Nb, and Le. The $\mathrm{Nu}_x\mathrm{Re}_x^{-1/2}$ is a rising function of parameters λ_2, γ, N, and Pr while being a declining function for λ, M, α_0, Nb, Nt, Ec, and Le. Moreover, the λ_2, γ, N, Nb, Ec, Pr, and Le tend to increase the $\mathrm{Sh}_x\mathrm{Re}_x^{-1/2}$ but λ, M, α_0, and Nt lead to the reduction of $\mathrm{Sh}_x\mathrm{Re}_x^{-1/2}$.

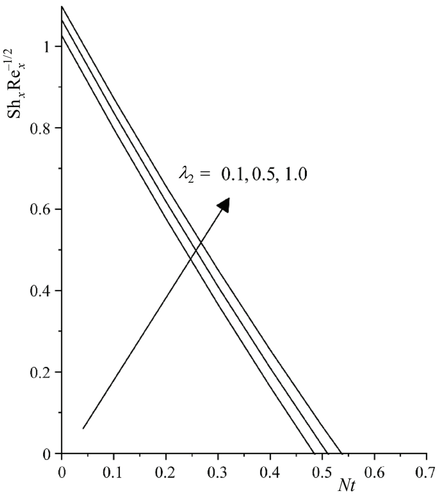

Figure 16. Impact of λ_2 and Nt on $Sh_x Re_x^{-1/2}$

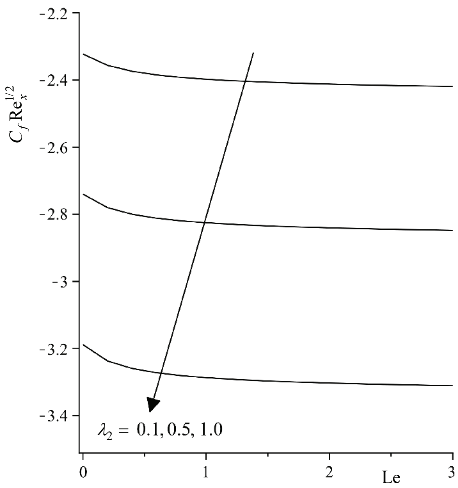

Figure 17. Impact of λ_2 and Le on $C_f Re_x^{1/2}$

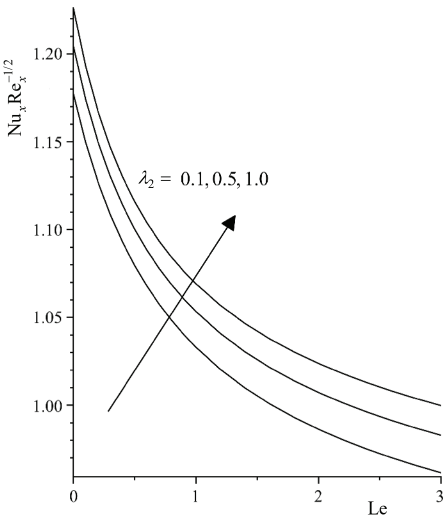

Figure 18. Impact of λ_2 and Le on $Nu_x Re_x^{-1/2}$

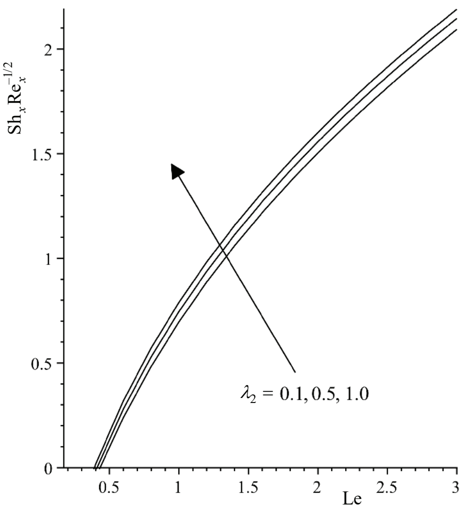

Figure 19. Impact of λ_2 and Le on $Sh_x Re_x^{-1/2}$

Conclusion

The influence of viscous dissipation on MHD mixed convection boundary-layer flow in a Jeffrey fluid induced by an inclined stretching sheet with nanoparticles has been tackled numerically. The flow dynamics of the regime have revealed to be controlled by the parameters λ, λ_2, N, Nb, Nt, Le, γ, M, and α_0. As a whole, the vital discoveries of this explorations are itemized as the following:

- Velocity profile is the accelerating function for λ_2, γ, and N while decelerating function for λ, M, and α_0.
- Temperature profile is the rising function for Nt, Nb, and Ec.

Table 2(a). Variations of $C_f \mathrm{Re}_x^{1/2}$, $\mathrm{Nu}_x \mathrm{Re}_x^{-1/2}$ and $\mathrm{Sh}_x \mathrm{Re}_x^{-1/2}$ for diverse values of λ, λ_2, M, γ, N, and α_0 when $\mathrm{Pr} = 1.0$, $Nb = Nt = 0.3$, $\mathrm{Ec} = 0.2$ and $\mathrm{Le} = 0.7$

λ	λ_2	M	γ	N	α_0	$C_f \mathrm{Re}_x^{1/2}$	$\mathrm{Nu}_x \mathrm{Re}_x^{-1/2}$	$\mathrm{Sh}_x \mathrm{Re}_x^{-1/2}$
0.1	0.2	0.7	0.3	0.3	π/4	–2.45467124	1.06364657	0.37800436
0.2						–2.34332358	1.05763770	0.36604793
0.6	0.2					–2.01004586	1.03595287	0.32880936
	0.4					–2.18409511	1.04803190	0.34860767
	0.8	0.7				–2.49821386	1.06588536	0.38273943
		0.8				–2.58145607	1.05522768	0.37706196
		1.0	0.3			–2.74143614	1.03452350	0.36681432
			0.5			–2.57603981	1.05887458	0.38234062
			1.0	0.3		–2.17834949	1.10827701	0.41119981
				0.5		–2.031877913	1.12712237	0.42503387
				1.0	π/6	–1.398056895	1.19127539	0.46620209
					π/5	–1.496720835	1.18300907	0.46144644
					π/4	–1.674055350	1.16717975	0.45246349

Table 2(b). Variations of $C_f \mathrm{Re}_x^{1/2}$, $\mathrm{Nu}_x \mathrm{Re}_x^{-1/2}$, and $\mathrm{Sh}_x \mathrm{Re}_x^{-1/2}$ for diverse values of Pr, Nb, Nt, Ec, and Le when $\lambda = 0.1$, $\lambda_2 = 0.2$, $M = 0.7$, $\gamma = N = 0.3$ and $\alpha_0 = \pi/4$

Pr	Nb	Nt	Ec	Le	$C_f \mathrm{Re}_x^{1/2}$	$\mathrm{Nu}_x \mathrm{Re}_x^{-1/2}$	$\mathrm{Sh}_x \mathrm{Re}_x^{-1/2}$
0.72	0.3	0.3	0.2	0.7	–2.43189716	0.91374296	0.26572697
1.0					–2.45467124	1.06364657	0.37800436
2.0	0.3				–2.50215862	1.35728324	0.83438782
	0.4				–2.50359559	1.27920429	1.06900570
	0.6	0.3			–2.50398200	1.13867823	1.29747410
		0.4			–2.49703951	1.10737407	1.21740740
		0.6	0.2		–2.48757790	1.05037240	1.07522236
			0.4		–2.48241908	0.94833203	1.15429927
			0.8	0.7	–2.47218203	0.74464535	1.31237355
				0.8	–2.47513636	0.72240831	1.47927916
				1.0	–2.47994315	0.68687867	1.77588553

- Concentration profile is the accelerating function for Nt while decreasing function for Nb and Lewis number.
- The rise in λ_2 and Lewis number has worsened the $C_f \mathrm{Re}_x^{1/2}$.
- For the increasing values of λ_2, Nt, and Le, the $\mathrm{Nu}_x \mathrm{Re}_x^{-1/2}$ and $\mathrm{Sh}_x \mathrm{Re}_x^{-1/2}$ are boosted.

Acknowledgment

This research is funded by Universiti Malaysia Pahang (RDU190356 and RDU1901124). The authors are therefore thankfully appreciative for the financial support.

Nomenclature

a, b, d, m, n – constants
B_0 – transverse magnetic field, [T]
C – nanoparticle concentration
C_∞ – ambient nanoparticle concentration
C_f – local skin friction coefficient
$C_f \mathrm{Re}_x^{1/2}$ – reduced skin friction coefficient
C_p – specific heat capacity at constant pressure, [Jkg^{-1}K^{-1}]

C_w – nanoparticle concentration at the surface
D_B – Brownian diffusion coefficient, [m^{2}s^{-1}]
D_T – thermophoretic diffusion coefficient, [m^{2}s^{-1}]
Ec – Eckert number, [–]
f – Dimensionless stream function, [ms^{-1}]
Gr – Grashof number, [–]
g – gravitational acceleration, [ms^{-2}]
k – thermal conductivity, [Wm^{-1}K^{-1}]
Le – Lewis number, [–]
M – magnetic parameter
N – concentration buoyancy parameter
Nb – Brownian motion parameter
Nt – thermophoresis parameter
Nu$_x$ – local Nusselt number, [–]
Nu$_x$Re$_x^{-1/2}$ – reduced Nusselt number, [–]
Pr – Prandtl number, [–]
p – pressure, [Pa]
q_m – surface mass flux
q_w – surface heat flux, [Wm^{-2}]
Re$_x$ – local Reynolds number, [–]
Sh$_x$ – local Sherwood number, [–]
Sh$_x$Re$_x^{-1/2}$ – reduced Sherwood number
T – fluid temperature, [K]
T_∞ – ambient temperature, [K]
T_w – wall temperature, [K]
u – velocity components along the x-direction, [ms^{-1}]
u_w – velocity of stretching sheet, [ms^{-1}]
v – velocity components along the y-direction, [ms^{-1}]

Greek Symbols

α – thermal diffusivity, [m^{2}s^{-1}]
α_0 – inclination angle, [rad]
β_C – concentration expansion coefficient
β_T – thermal expansion coefficient, [K^{-1}]
γ – mixed convection parameter
η – similarity variable
η_∞ – boundary-layer thickness
θ – dimensionless temperature, [–]
λ – ratio of relaxation and retardation time
λ_1 – retardation time
λ_2 – Deborah number
μ – dynamic viscosity, , [kgm^{-1}s^{-1}]
ρ_f – density of fluid, [kgm^{-3}]
σ – electrical conductivity, [Sm^{-1}]
τ – ratio of heat capacity of nanoparticle to the base fluid
$\boldsymbol{\tau}_w$ – surface shear stress, [kgm^{-1}s^{-2}]
ϕ – rescaled nanoparticle concentration
ν – kinematic viscosity, [m^{2}s^{-1}]

Subscripts

∞ – condition at the free stream
f – fluid
p – nanoparticle material
w – condition at the wall

Superscripts

$'$ – differentiation with respect to η

References

[1] Kasim, A. R. M., *et al.*, Constant Heat Flux Solution for Mixed Convection Boundary Layer Viscoelastic Fluid, *Heat and Mass Transfer*, *49* (2013), 2, pp. 163-171
[2] Anwar, M., *et al.*, Numerical Study for MHD Stagnation-Point Flow of a Micropolar Nanofluid Towards a Stretching Sheet, *Journal of the Brazilian Society of Mechanical Sciences and Engineering*, *39* (2017), 1, pp. 89-100
[3] Hashim, *et al.*, Numerical Investigation on Time-Dependent Flow of Williamson Nanofluid Along with Heat and Mass Transfer Characteristics Past a Wedge Geometry, *International Journal of Heat and Mass Transfer*, *118* (2018), Mar., pp. 480-491
[4] Zokri, S. M., *et al.*, Influence of Viscous Dissipation on the Flow and Heat Transfer of a Jeffrey Fluid Towards Horizontal Circular Cylinder with Free Convection: A Numerical Study, *Malaysian Journal of Fundamental and Applied Sciences*, *14* (2018), 1, pp. 40-47
[5] Hayat, T., *et al.*, Mixed Convection Flow of Viscoelastic Nanofluid over a Stretching Cylinder, *Journal of the Brazilian Society of Mechanical Sciences and Engineering*, *37* (2015), 3, pp. 849-859
[6] Dalir, N., Numerical Study of Entropy Generation for Forced Convection Flow and Heat Transfer of a Jeffrey Fluid over a Stretching Sheet, *Alexandria Engineering Journal*, *53* (2014), 4, pp. 769-778
[7] Hayat, T., *et al.*, Unsteady Flow and Heat Transfer of Jeffrey Fluid over a Stretching Sheet, *Thermal Science*, *18* (2014), 4, pp. 1069-1078
[8] Narayana, P. V. S., Babu, D. H., Numerical Study of MHD Heat and Mass Transfer of a Jeffrey Fluid over a Stretching Sheet with Chemical Reaction and Thermal Radiation, *Journal of the Taiwan Institute of Chemical Engineers*, *59* (2016), 2016, Feb., pp. 18-25
[9] Ojjela, O., *et al.*, Influence of Thermophoresis and Induced Magnetic Field on Chemically Reacting Mixed Convective Flow of Jeffrey Fluid between Porous Parallel Plates, *Journal of Molecular Liquids*,

232 (2017), Apr., pp. 195-206
[10] Hayat, T., *et al.*, Cattaneo-Christov Double-Diffusion Model for Flow of Jeffrey Fluid, *Journal of the Brazilian Society of Mechanical Sciences and Engineering*, *39* (2017), 12, pp. 4965-4971
[11] Hayat, T., *et al.*, Effect of Cattaneo-Christov Heat Flux on Jeffrey Fluid Flow with Variable Thermal Conductivity, *Results in Physics*, *8* (2018), Mar., pp. 341-351
[12] Choi, S. U., Eastman, J. A., Enhancing Thermal Conductivity of Fluids with Nanoparticles, Report no. 84938, San Francisco, Cal., USA, 1995
[13] Buongiorno, J., Convective Transport in Nanofluids, *Journal of Heat Transfer*, *128* (2006), 3, pp. 240-250
[14] Eastman, J. A., *et al.*, Anomalously Increased Effective Thermal Conductivities of Ethylene Glycol-based Nanofluids Containing Copper Nanoparticles, *Applied Physics Letters*, *78* (2001), 6, pp. 718-720
[15] Choi, S., *et al.*, Anomalous Thermal Conductivity Enhancement in Nanotube Suspensions, *Applied Physics Letters*, *79* (2001), 14, pp. 2252-2254
[16] Khan, W., Pop, I., Boundary-layer Flow of a Nanofluid past a Stretching Sheet, *International Journal of Heat and Mass Transfer*, *53* (2010), 11, pp. 2477-2483
[17] Makinde, O. D., Aziz, A., Boundary Layer Flow of a Nanofluid past a Stretching Sheet with a Convective Boundary Condition, *International Journal of Thermal Sciences*, *50* (2011), 7, pp. 1326-1332
[18] Ibrahim, W., Makinde, O., Magnetohydrodynamic Stagnation Point Flow of a Power-Law Nanofluid Towards a Convectively Heated Stretching Sheet with Slip, *Proceedings of the Institution of Mechanical Engineers, Part E: Journal of Process Mechanical Engineering*, *230* (2016), 5, pp. 345-354
[19] Shehzad, S. A., *et al.*, Thermally Radiative Three-dimensional Flow of Jeffrey Nanofluid with Internal Heat Generation and Magnetic Field, *Journal of Magnetism and Magnetic Materials*, *397* (2016), Jan., pp. 108-114
[20] Avinash, K., *et al.* Non-Uniform Heat Source/Sink Effect on Liquid Film Flow of Jeffrey Nanofluid over a Stretching Sheet, *Diffusion Foundations, 11* (2017), Aug., pp. 72-83
[21] Qayyum, S., *et al.*, Magnetohydrodynamic (MHD) Nonlinear Convective Flow of Jeffrey Nanofluid over a Nonlinear Stretching Surface with Variable Thickness and Chemical Reaction, *International Journal of Mechanical Sciences*, *134* (2017), Dec., pp. 306-314
[22] Abbasi, F., *et al.*, Mixed Convection Flow of Jeffrey Nanofluid with Thermal Radiation and Double Stratification, *Journal of Hydrodynamics, Ser. B*, *28* (2016), 5, pp. 840-849
[23] Dhanai, R., *et al.*, MHD Mixed Convection Nanofluid Flow and Heat Transfer over an Inclined Cylinder due to Velocity and Thermal Slip Effects: Buongiorno's Model, *Powder Technology*, *288* (2016), Jan., pp. 140-150
[24] Sakiadis, B., Boundary-layer Behavior on Continuous Solid Surfaces: I. Boundary-layer Equations for Two-dimensional and Axisymmetric Flow, *AIChE Journal*, *7* (1961), 1, pp. 26-28
[25] Crane, L. J., Flow Past a Stretching Plate, *Zeitschrift für Angewandte Mathematik und Physik (ZAMP)*, *21* (1970), 4, pp. 645-647
[26] Makinde, O., *et al.*, MHD Flow of a Variable Viscosity Nanofluid over a Radially Stretching Convective Surface with Radiative Heat, *Journal of Molecular Liquids*, *219* (2016), July, pp. 624-630
[27] Salleh, M. Z., *et al.*, Boundary Layer Flow and Heat Transfer over a Stretching Sheet with Newtonian Heating, *Journal of the Taiwan Institute of Chemical Engineers*, *41* (2010), 6, pp. 651-655
[28] Mamatha, S., *et al.* Effect of Convective Boundary Condition on MHD Carreau Dusty Fluid over a Stretching Sheet with Heat Source, *Defect and Diffusion Forum*, *377* (2017), Sept., pp. 233-241.
[29] Hsiao, K.-L., Stagnation Electrical MHD Nanofluid Mixed Convection with Slip Boundary on a Stretching Sheet, *Applied Thermal Engineering*, *98* (2016), Apr., pp. 850-861
[30] Reddy, P. B. A., Magnetohydrodynamic Flow of a Casson Fluid over an Exponentially Inclined Permeable Stretching Surface with Thermal Radiation and Chemical Reaction, *Ain Shams Engineering Journal*, *7* (2016), 2, pp. 593-602
[31] Afridi, M. I., *et al.*, Entropy Generation in Magnetohydrodynamic Mixed Convection Flow over an Inclined Stretching Sheet, *Entropy*, *19* (2016), 1, pp. 10
[32] Sravanthi, C., Homotopy Analysis Solution of MHD Slip Flow past an Exponentially Stretching Inclined Sheet with Soret-Dufour Effects, *Journal of the Nigerian Mathematical Society*, *35* (2016), 1, pp. 208-226
[33] Thumma, T., *et al.*, Numerical Study of Heat Source/Sink Effects on Dissipative Magnetic Nanofluid Flow from a Non-Linear Inclined Stretching/Shrinking Sheet, *Journal of Molecular Liquids*, *232* (2017), Apr., pp. 159-173
[34] Gupta, S., *et al.*, MHD Mixed Convective Stagnation Point Flow and Heat Transfer of an Incompressible Nanofluid over an Inclined Stretching Sheet with Chemical Reaction and Radiation, *International Journal*

of Heat and Mass Transfer, *118* (2018), Mar., pp. 378-387
[35] Soundalgekar, V., Viscous Dissipation Effects on Unsteady Free Convective Flow past an Infinite, Vertical Porous Plate with Constant Suction, *International Journal of Heat and Mass Transfer*, *15* (1972), 6, pp. 1253-1261
[36] Yirga, Y., Shankar, B., Effects of Thermal Radiation and Viscous Dissipation on Magnetohydrodynamic Stagnation Point Flow and Heat Transfer of Nanofluid towards a Stretching Sheet, *Journal of Nanofluids*, *2* (2013), 4, pp. 283-291
[37] Mohamed, M. K. A., *et al.*, Effects of Viscous Dissipation on Free Convection Boundary Layer Flow towards a Horizontal Circular Cylinder, *ARPN Journal of Engineering and Applied Sciences*, *11* (2016), 11, pp. 7258-7263
[38] Mohamed, M. K. A., *et al.*, The Viscous Dissipation Effects on The Mixed Convection Boundary Layer Flow on a Horizontal Circular Cylinder, *Jurnal Teknologi*, *78* (2016), 4-4, pp. 73-79
[39] Besthapu, P., *et al.*, Mixed Convection Flow of Thermally Stratified MHD Nanofluid over an Exponentially Stretching Surface with Viscous Dissipation Effect, *Journal of the Taiwan Institute of Chemical Engineers*, *71* (2017), Feb., pp. 307-314
[40] Hussain, A., *et al.*, Combined Effects of Viscous Dissipation and Joule Heating on MHD Sisko Nanofluid over a Stretching Cylinder, *Journal of Molecular Liquids*, *231* (2017), Apr., pp. 341-352
[41] Kumar, R., *et al.*, Rotating Frame Analysis of Radiating and Reacting Ferro-nanofluid Considering Joule heating and Viscous Dissipation, *International Journal of Heat and Mass Transfer*, *120* (2018), May, pp. 540-551
[42] Mahanthesh, B., Gireesha, B. J., Scrutinization of Thermal Radiation, Viscous Dissipation and Joule Heating Effects on Marangoni Convective Two-phase Flow of Casson Fluid with Fluid-particle Suspension, *Results in Physics*, *8* (2018), Mar., pp. 869-878
[43] Makinde, O., Olanrewaju, P., Buoyancy Effects on Thermal Boundary Layer over a Vertical Plate with a Convective Surface Boundary Condition, *Journal of Fluids Engineering*, *132* (2010), 4, pp. 044502
[44] Makinde, O. D., Similarity Solution for Natural Convection from a Moving Vertical Plate with Internal Heat Generation and a Convective Boundary Condition, *Thermal Science*, *15* (2011), suppl. 1, pp. 137-143
[45] Afridi, M. I., *et al.*, Entropy Generation in Hydromagnetic Boundary Flow under the Effects of Frictional and Joule Heating: Exact Solutions, *The European Physical Journal Plus*, *132* (2017), 9, 404
[46] Rauf, A., *et al.*, MHD Stagnation Point Flow of Micro Nanofluid towards a Shrinking Sheet with Convective and Zero Mass Flux Conditions, *Bulletin of the Polish Academy of Sciences Technical Sciences*, *65* (2017), 2, pp. 155-162
[47] Chaudhary, R. C., Jain, P., An Exact Solution to the Unsteady Free-convection Boundary-layer Flow past an Impulsively Started Vertical Surface with Newtonian Heating, *Journal of Engineering Physics and Thermophysics*, *80* (2007), 5, pp. 954-960
[48] Reddy, P. S., *et al.*, MHD Heat and Mass Transfer Flow of a Nanofluid over an Inclined Vertical Porous Plate with Radiation and Heat Generation/Absorption, *Advanced Powder Technology*, *28* (2017), 3, pp. 1008-1017

Paper submitted: November 20, 2017
Paper revised: June 18, 2018
Paper accepted: June 23, 2018